energies

MDPI

Article

A Self-Contained Electro-Hydraulic Cylinder with Passive Load-Holding Capability

Damiano Padovani [1,*], Søren Ketelsen [2], Daniel Hagen [1] and Lasse Schmidt [2]

[1] Department of Engineering Sciences, University of Agder, 4879 Grimstad, Norway; daniel.hagen@uia.no
[2] Department of Energy Technology, Aalborg University, 9220 Aalborg East, Denmark; sok@et.aau.dk (S.K.); lsc@et.aau.dk (L.S.)
* Correspondence: damiano.padovani@uia.no; Tel.: +47-37233020

Received: 21 December 2018; Accepted: 15 January 2019; Published: 18 January 2019

Abstract: Self-contained electro-hydraulic cylinders have the potential to replace both conventional hydraulic systems and the electro-mechanical counterparts enhancing energy efficiency, plug-and-play installation, and reduced maintenance. Current commercial solutions of this technology are limited and typically tailor-made, whereas the research emphasis is primarily on cost efficiency and power applications below five [kW]. Therefore, there is the need of developing more flexible systems adaptable to multiple applications. This research paper offers a contribution in this regard. It presents an electro-hydraulic self-contained single-rod cylinder with passive load-holding capability, sealed tank, capable of recovering energy, and scalable up to about eighty [kW]. The system implementation on a single-boom crane confirms its feasibility: The position tracking error remains well within ± 2 [mm], oscillations are limited, and the overall energy efficiency is about 60 [%] during actuation. Concerning the passive load-holding devices, it is shown that both vented and non-vented pilot-operated check valves achieve the desired functioning and can hold the actuator position without consuming energy. Additional observations about the size and the arrangement of the load-holding valves are also provided. In conclusion, this paper demonstrates that the proposed self-contained cylinder can be successfully extended to several practical applications, especially to those characterized by overrunning external loads and the need of securing the actuator position.

Keywords: Self-contained cylinders; electro-hydraulic systems; load-holding valves; modeling

1. Introduction

Linear actuators capable of delivering high forces to perform heavy-duty operations are commonplace in many fields of industry. Lifters, earth-moving or construction machines, manufacturing processes, and oil drilling applications are a few examples. Since energy efficiency, plug-and-play installation, and reduced maintenance are becoming crucial characteristics in these areas, there is an ongoing tendency to replace standard valve-controlled hydraulic cylinders with the electro-mechanical counterparts (e.g., roller-screw actuators directly driven by electric motors [1]). Nevertheless, these electro-mechanical solutions are unsuitable in several applications such as offshore oil drilling [2], mainly due to the limited reliability (i.e., unexpected impact forces and overloads damage the screw). An alternative approach makes use of self-contained electro-hydraulic cylinders (SCCs). They are, according to the definition used in this paper, self-sufficient linear hydraulic actuators controlled by a local hydraulic unit that is driven by a dedicated electric motor. A sealed tank is essential and additional components such as flow balancing valves and load-holding valves might be required. Figure 1 provides a simplified example of a SCC, even though multiple system architectures are conceivable. More in general, this approach intends to:

- Ensure high energy efficiency (i.e., suitable hydraulic layouts are chosen),

- Achieve compactness (i.e., the built-in components are arranged ad hoc),
- Allow plug-and-play commissioning (i.e., the system only requires a wired connection to the electrical power source),
- Enhance flexible installation (i.e., a centralized hydraulic power supply is not required anymore, long hydraulic transmission lines are removed, and the closed-circuit layout characterized by a sealed reservoir can be tilted without leaking out fluid).

Countless applications will benefit from such a drive solution. A few examples are cranes, presses, gripper arms for offshore pipe handling, marine jack plates, trailer lifts, scissors tables, positioning systems for solar panels, and Stewart platforms.

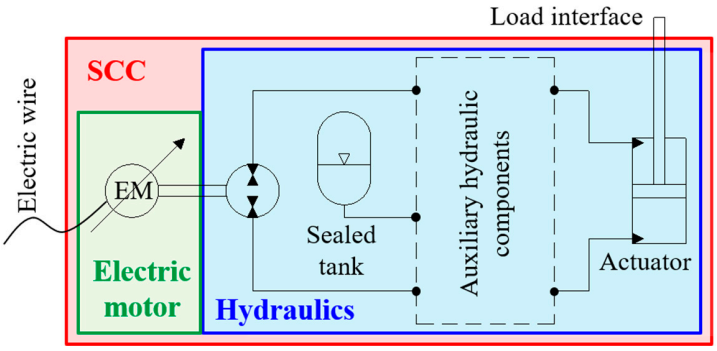

Figure 1. Simplified illustration of a self-contained electro-hydraulic cylinder.

In regard to what has been done so far, a limited number of commercial SCCs were introduced to the market, mainly using single-rod cylinders [3]; those are typically tailor-made solutions restricted to some niche applications because exceptional design effort is needed. It is the authors' opinion that this circumscribed use of SCCs is mainly due to the lack of consistent investigations aimed at identifying cost-effective system architectures adaptable to multiple applications.

Concerning the research activities connected to SCCs, emphasis is primarily on cost efficiency [4], thermal behavior [5], and low power applications below 5 [kW] [6,7]. Employing valve-less architectures to control the hydraulic actuators is commonplace since higher energy efficiency is achieved. Scenarios involving passive load-holding capability (i.e., maintaining the piston position without delivering any power) are seldom addressed, as shown in the next section. There is, therefore, the need of developing a SCC adaptable to the changing requirements of multiple applications and sustainable as a valid alternative to electro-mechanical systems.

This research paper presents a system architecture for an electro-hydraulic self-contained single-rod cylinder in closed-circuit configuration with passive load-holding capability, sealed tank, capable of recovering energy, and suitable for power levels above 5 [kW] representative of many hydraulic machines. Effort is dedicated to motivating the introduction of such a system, to experimentally confirm that the desired performance is achieved in terms of both actuator's position tracking and energy efficiency, and to better understanding the load load-holding capability (insight on the design of the load-holding valves and on their settings is given as well as on their arrangement in the hydraulic layout). This work significantly extends a previous conference publication [8] where a numerical analysis of a SCC that meets the aforementioned requirements is proposed. Specifically, this paper makes the following novel contributions: An improved system architecture, the implementation of the SCC on a test-bed, the experimental validation of the proposed dynamic model, the analysis of the system performance, and noteworthy considerations about the load-holding valves not traced in the technical literature.

2. Literature Survey

Due to the limited literature on SCCs, this survey also covers generic valve-less systems that might be converted into self-contained solutions. The main reason for focusing on valve-less layouts is

their potential for high energy efficiency (i.e., throttle-related losses in control valves are removed and energy recovery can be easily implemented). In fact, conventional valve-controlled systems waste a considerable percentage of the input energy in control valves (e.g., about 35 [%] in working cycles of load-sensing excavators [9]). Previous investigations about throttle-less concepts showed fuel savings up to 40 [%] in comparison to standard hydraulics [10].

Relevant valve-less systems that drive linear actuators can be classified depending on the following closed-circuit layouts:

1. Variable-displacement hydraulic unit and fixed-speed prime mover. The actuator motion is controlled by varying the displacement of the hydraulic pump/motor. This approach is prevalent among multi-actuator machines (e.g., compact excavators [10]) since a unique charge pump supplies the displacement adjustment system of each unit. The prime mover can be either a combustion engine or an electric motor.
2. Fixed-displacement hydraulic unit and variable-speed prime mover. Regulating both the angular speed and the direction of rotation of the prime mover's shaft controls the actuator motion [3,11–13]. The electric prime mover can be either a synchronous machine [11] or an asynchronous machine [14].
3. Variable-displacement hydraulic unit and variable-speed prime mover. Both the electric prime mover and the hydraulic unit actively control the actuator motion [15].

Narrowing the search field to case #2, this approach minimizes the number of control elements when compared to case #3 (i.e., a much cheaper fixed-displacement hydraulic unit is selected) and simplifies the hydraulics if related to case #1 (i.e., the pressure source dedicated to adjusting the unit displacement is not needed).

Moreover, a competing valve-less solution that does not fall under any of these three categories is gaining ground. It is based on multiple fixed-displacement pumps/motors driven by a common variable-speed prime mover. Alternatives with two hydraulic units [6,16–18] or with three hydraulic units [19–21] exist.

Regarding the hydraulic actuator, double-rod cylinders are almost exclusively used in the aerospace industry [22–26]. When compared to the single-rod design, the double-rod configuration increases the installation space and delivers a reduced output force for a given pressure. Thus, single-rod cylinders are the most popular solution for at least 80% of the electro-hydraulic drives [27]. Balancing the differential flow dictated by the unequal piston areas is, therefore, essential to implement a closed-circuit architecture. Various flow compensation methods were investigated in the past, mainly involving pilot-operated check valves [28], shuttle valves [13], or electrically-operated on/off valves [29]. Some issues related to instability and uncontrolled pressure oscillations were mentioned for shuttle valves [13] and for pilot-operated check valves [30], respectively. However, this is typically the case under high dynamic excitations of the system [3] (i.e., operating conditions that might be representative of some low-power applications). Other flow compensation alternatives were explored such as hydraulic transformers, three-port asymmetric piston pumps, or multiple gear pumps. Table 1 provides a synthesis of these options.

Table 1. Methods for compensating the differential flow.

Methods	References
Hydraulic transformers	[31–33]
Pilot-operated check valves	[10,28,34–38]
Inverse shuttle valve	[3,39,40]
3-port asymmetric pump	[41–44]
Two cylinders in parallel	[45]
Multiple fixed-displacement pumps	[6,16–21,46]

Additionally, limited researches addressed passive load-holding capabilities for SCCs. This feature serves the purpose of maintaining a given actuator position without supplying any power to the system.

A first solution is a commercialized system [47,48] where pilot-operated check valves (POCVs) are installed between the pump and the actuator. The hydraulic connections are arranged in such a manner that each opening pilot line of the POCVs is sensing the pressure of the opposite pump side. A similar approach is also presented in Reference [49]. Then, an interesting method to control the opening pilot of POCVs is discussed in References [37,38] and in Reference [50], even though this technique is not intended for SCCs. Alternatively, passive load-holding systems grounded on counterbalance valves were studied in Reference [12] and References [51,52], but they cannot recover energy.

Table 2 summarizes the system architectures for the SCCs addressed in this survey. Details about the presence of the passive load-holding capability (P_{LH}) are listed, as well as the possibility of performing four quadrant operations (4Q) that refer to piston extension and to piston retraction with both resistant and overrunning external loads acting on the actuator.

Table 2. Self-contained cylinders: concepts and characteristics.

Architectures	4Q	P_{LH}	References
Multiple fixed-displacement pumps	No	No	[27]
Multiple fixed-displacement pumps	Yes	No	[11,20,21]
Inverse shuttle valves	Yes	No	[3,5,6,13,53]
Compact system	Yes [1]	Yes	[12,51]
Electro-hydraulic actuator	No	Yes	[47–49]

[1] No energy recovery.

In conclusion, the idea behind electro-hydraulic self-contained cylinders is to combine the advantages of standard hydraulic actuators (i.e., reliability and high power-to-weight ratio) with the benefits of electro-mechanical drives (i.e., energy efficiency, minimal maintenance, and simple plug-and-play commissioning). Extra requirements such as compactness, robustness, and reduced costs are also of interest due to their relevance in both industrial and mobile applications [3,17].

3. The System under Investigation

According to the literature review, the requirements for SCCs listed in the introduction are not met by previously published solutions (several systems only represent a partial fit according to Table 2). Hence, some of these features were combined accordingly to create the proposed SCC.

3.1. System Architecture

Figure 2 depicts the self-contained cylinder discussed in this investigation. The system operates in four quadrants, includes passive load-holding devices, can recover energy, has a sealed reservoir, and is suitable for power levels up to at least 80 [kW].

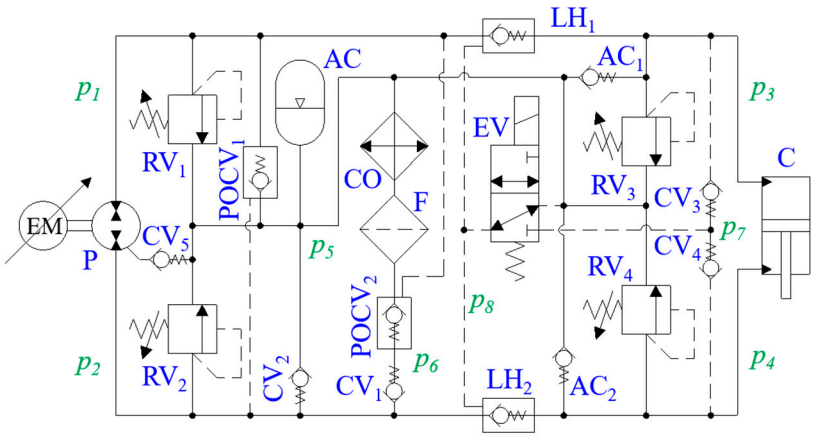

Figure 2. System architecture of the investigated self-contained cylinder.

The combination of an electric servo-motor (EM) and of a fixed-displacement hydraulic unit (P) drives the single-rod double-acting cylinder (C) arranged in a closed-circuit configuration. The differential flow dictated by the piston's unequal areas is balanced by two pilot-operated check valves ($POCV_{1\to2}$) and by two check valves ($CV_{1\to2}$). The low-pressure accumulator (AC) represents the sealed reservoir of the SCC. The pilot-operated check valves LH_1 and LH_2 (i.e., the load-holding valves) create the passive load-holding capability by isolating the actuator when the 3/2 electro-valve (EV) is de-energized. Conversely, energizing the EV results in transferring the highest actuator pressure into the opening pilot line of the two load-holding valves (the check valves $CV_{3\to4}$ select the dominant value among the pressures in the cylinder chambers); this enables the actuator motion. As can be seen, the EV is repositioned by the spring force in case of power failure, securing the load-holding function. Pressure-relief valves ($RV_{1\to4}$) are installed on both pump ports and on both actuator ports to avoid over-pressurizations during actuation and throughout passive load-holding. Anti-cavitation valves ($AC_{1\to2}$) are also connected to the actuator chambers. A cooler (CO) and a filter (F) are comprised in the system. The cooler can be easily removed if it is not necessary.

Figure 3 takes advantage of a simplified system representation to outline the operating condition in each quadrant when the passive load-holding capability is deactivated (i.e., EV is energized). Flow directions and pressure levels are emphasized: The red color denotes the high-pressure side, the blue color designates the low-pressure side, Q_p is the cylinder flow on the bore-side, Q_r is the cylinder flow on the rod-side, and $Q_d = Q_p - Q_r$ represents the differential flow. For a given speed of the servo-motor, the actuator velocity is higher in the left half-plane because the pump/motor flow is going to (or is coming from) the actuator's rod-side chamber that has a smaller piston area than the bore-side. More importantly, it should be noted that this system architecture fits particularly well with applications characterized by frequent overrunning loads acting on the actuator (e.g., cranes); the differential flow is, in fact, forced to go through both the filter and the cooler during operations in the IV quadrant, ensuring proper fluid conditioning.

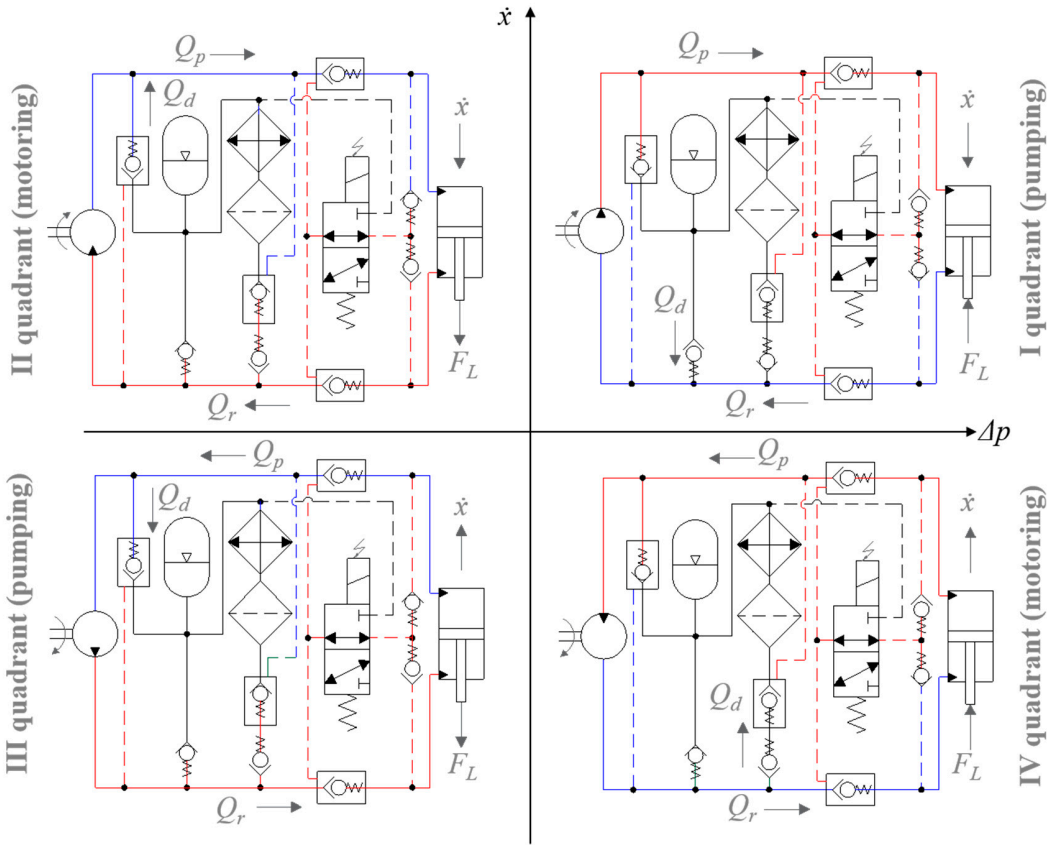

Figure 3. Simplified illustration of the system functioning in four quadrants ($\Delta p = p_1 - p_2$).

3.2. Control Algorithm

The control algorithm designed for this SCC generates a reference speed for the electric servo-motor in order to track the commanded position of the linear actuator. The control logic emerges from the block diagram proposed in Figure 4. A feedforward controller (FF) estimates the required servo-motor speed (u_{FF}) via (1), depending on the operating condition (there are different formulations for each quadrant). The actuator's bore-side area (A_p), the rod-side area (A_r), the pump/motor displacement (D), and a constant volumetric efficiency (e.g., $\eta_v = 0.95$ in motoring mode and $\eta_v = 1$ in pumping mode) are recalled.

$$u_{FF} = \begin{cases} \frac{\dot{x}_{Set} \cdot A_p}{D \cdot \eta_v} & \text{if } \dot{x} \geq 0 \;\&\; \Delta p \geq 0 \quad \text{(i.e., I quadrant)} \\ \frac{\dot{x}_{Set} \cdot A_r \cdot \eta_v}{D} & \text{if } \dot{x} \geq 0 \;\&\; \Delta p < 0 \quad \text{(i.e., II quadrant)} \\ \frac{\dot{x}_{Set} \cdot A_r}{D \cdot \eta_v} & \text{if } \dot{x} < 0 \;\&\; \Delta p < 0 \quad \text{(i.e., III quadrant)} \\ \frac{\dot{x}_{Set} \cdot A_p \cdot \eta_v}{D} & \text{if } \dot{x} < 0 \;\&\; \Delta p \geq 0 \quad \text{(i.e., IV quadrant)} \end{cases} \tag{1}$$

The proportional-integral controller (PI) in the position feedback loop corrects the prediction of the feedforward term by manipulating the position error (e_x). The proportional gain $k_P = 90$ [rev/(min·mm)] and the integral gain $k_I = 300$ [rev/(min·mm·s)] generate the corresponding feedback command (u_{FB}).

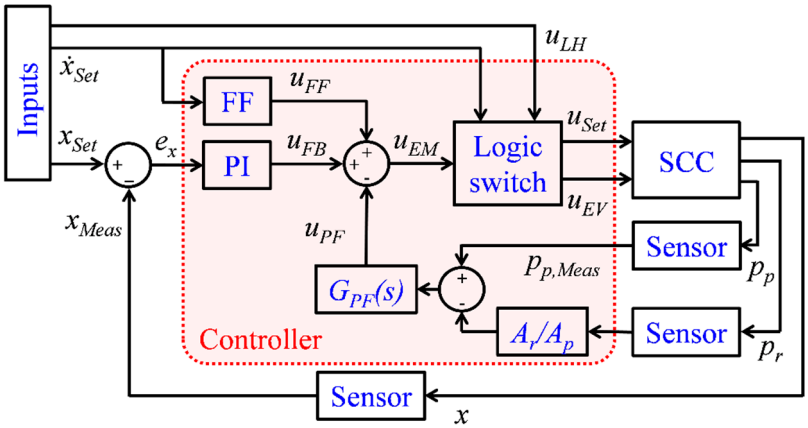

Figure 4. Block diagram of the control algorithm.

Additionally, a negative pressure feedback term (u_{PF}) adds damping to the system by canceling out pressure oscillations. This is done by filtering the measured actuator pressures using a first-order high-pass filter (2). Its cut-off frequency is $\omega_{PF} = 3$ [rad/s], whereas the small filter gain $k_{PF} = 5 \times 10^{-5}$ [rev/min/Pa] is due to the input being [Pa].

$$G_{PF}(s) = k_{PF} \cdot \frac{s}{s + \omega_{PF}} \tag{2}$$

The resulting speed command for the servo-motor (u_{EM}) is then sent through the logic switch and finally propagated to the SCC. The logic switch sets the commanded motor speed (u_{Set}) to zero when actuator motion is not desired (i.e., when $|\dot{x}_{Set}| < 0.005$ [mm/s]) otherwise it does not affect the signal. At the same time, the logic switch generates the command (u_{EV}) directed to the 3/2 electro-valve that engages, or disengages, the load-holding capability. If the load-holding enabler (u_{LH}) is active (this means passive load-holding is wanted), then the EV is energized when $\dot{x}_{Set}$ is non-zero or de-energized when $\dot{x}_{Set}$ is zero and the position error is smaller than two [mm]. If passive load-holding is not desired (i.e., u_{LH} is switched off), then the EV is energized independently of $\dot{x}_{Set}$.

4. Experimental Set-Up

An experimental test-bed was commissioned to drive a single-boom crane available at the University of Agder (Figure 5). This representative application was selected since it encompasses different operating conditions such as motion against both resistant external loads (i.e., I quadrant) and overrunning external loads (i.e., IV quadrant). It also offers the opportunity of testing the passive load-holding capability. Furthermore, this crane challenges the performance of the SCC because the mechanical structure was specifically designed to enhance oscillations (originally, the crane was driven by a valve-controlled system [54]). More details about the crane are available in Appendix A.

Regarding the SCC, the selected servo-motor is a PMSM Bosch Rexroth MSK071E-0300 with a dedicated driver IndraDrive HCS02. The axial-piston swashplate unit A10F has a displacement of 10.6 [cm^3/rev]. The cylinder PMC 25CA has piston diameter of 65 [mm], rod diameter of 35 [mm], and stroke of 500 [mm]. The load-holding valves (Sun Hydraulics CVEVXFN) have area ratio 3:1 and cracking pressure of seven [bar], whereas the other POCVs (Sun Hydraulics CKEBXCN) have the same area ratio, but cracking pressure of two [bar]. The opening pilot for the load-holding valves is selected by means of check valves Hawe Hydraulics RB2 with cracking pressure of 0.1 [bar] and of a 3/2 directional control valve Argo Hytos SD1E. The additional check valves Hawe Hydraulic RK4 still have cracking pressure of 0.1 [bar], whereas the pressure-relief valves Sun Hydraulics RDDA have cracking pressure of 200 [bar]. A tailor-made manifold houses these valves. A Bosch Rexroth cooler KOL3N (cooling power up to 3 [kW]) and a filter 50LEN0100 are used to condition the oil ISO VG 46.

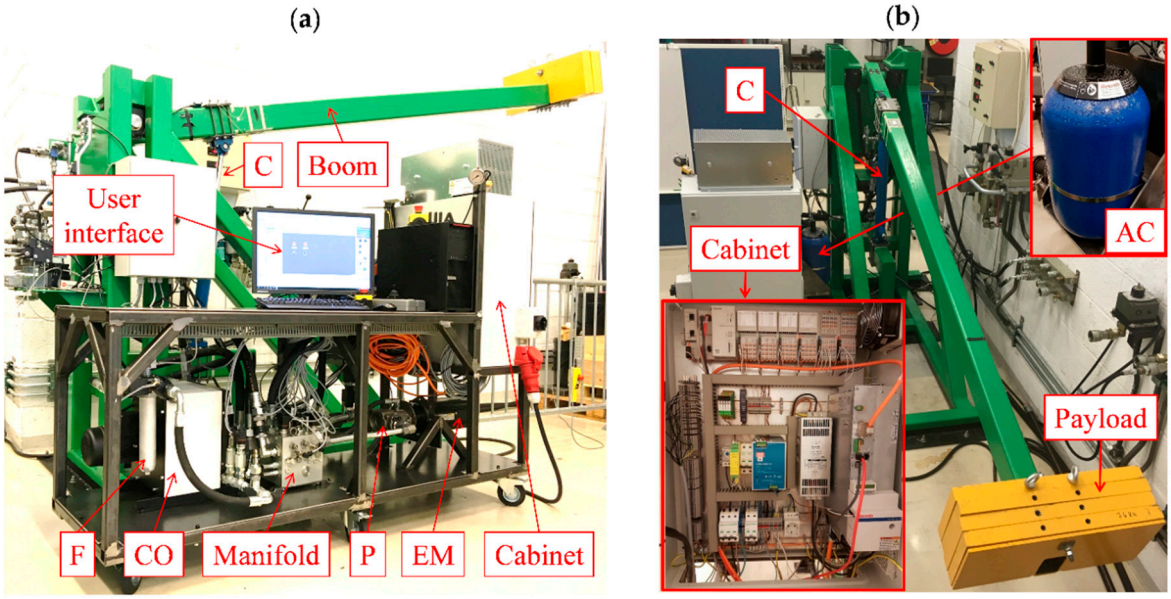

Figure 5. (**a**) Overview of the experimental test-bed; and (**b**) detailed view of the single-boom crane and of the electric cabinet dedicated to the servo-motor.

In terms of sensors, the servo-motor comes standard with an encoder. A position sensor Regal PS6310 monitors the actuator's piston position. Transducers Bosch Rexroth HM20 measure the pressures $p_{1\to5}$. Finally, MATLAB-Simulink®is used for control and data acquisition. The software IndraWorks translates the control algorithm into machine code that runs at a frequency of 1000 [Hz] on the PLC IndraControl XM22.

5. System Modeling and Validation

Multiple dynamic models of the SCC were created and simulated in MATLAB-Simulink®.

5.1. The Dynamic Modeling of the System

The electric servo-motor was modeled using a second-order transfer function (3) from commanded to simulate shaft speed where the natural frequency and the damping ratio are ω_n = 5 [Hz] and ζ = 0.99, respectively.

$$G_{EM}(s) = \frac{\omega_n^2}{s^2 + 2 \cdot \omega_n \cdot \zeta \cdot s + \omega_n^2} \tag{3}$$

The hydraulics was simulated by means of a consolidated approach. The effective fluid's bulk modulus (β_i) in the i-th hydraulic capacitance was modeled via Equation (4).

$$\beta_i = \frac{1}{\frac{1}{\beta_O} + \varepsilon_{A,i} \cdot \left(\frac{1}{\beta_{A,i}} - \frac{1}{\beta_O} \right)} \tag{4}$$

The different terms are the oil's bulk modulus (β_O = 7500 [bar]), the air's bulk modulus ($\beta_{A,i}$) calculated as $\beta_{A,i} = \gamma \cdot p_i$ with γ being the adiabatic air constant and p_i the pressure in the capacitance, and the volumetric air content ($\varepsilon_{A,i}$), which is obtained according to Equation (5). This equation recalls the atmospheric pressure (p_{atm}) and the volumetric air content of the oil at atmospheric pressure ($\varepsilon_{A,0}$ = 0.015 [%]).

$$\varepsilon_{A,i} = \frac{1}{\frac{1-\varepsilon_{A,0}}{\varepsilon_{A,0}} \cdot \left(\frac{p_{atm}}{p_i} \right)^{-\frac{1}{\gamma}} + 1} \tag{5}$$

The well-known pressure build-up equation was applied several times to evaluate the pressures $p_{1 \to 8}$ labeled in Figure 2. The resulting expressions are reported in Equations (6)–(13) where the effective bulk modulus (β_i), the appropriate flow rates (Q_i), and the suitable volumes of the hydraulic capacitances (V_i) are considered accordingly.

$$\dot{p}_1 = \frac{\beta_1 \cdot (Q_{e,P} + Q_{POCV,1} - Q_{LH,1} - Q_{RV,1})}{V_{1,0}} \tag{6}$$

$$\dot{p}_2 = \frac{\beta_2 \cdot (-Q_{e,P} - Q_{CV,1} + Q_{CV,2} - Q_{LH,2} - Q_{RV,2})}{V_{2,0}} \tag{7}$$

$$\dot{p}_3 = \frac{\beta_3 \cdot (Q_{LH,1} - A_p \cdot \dot{x} - Q_{RV,3} + Q_{AC,1} - Q_{CV,3})}{V_{3,0} + A_p \cdot x} \tag{8}$$

$$\dot{p}_4 = \frac{\beta_4 \cdot (Q_{LH,2} + A_r \cdot \dot{x} - Q_{RV,4} + Q_{AC,2} - Q_{CV,4})}{V_{4,0} + A_r \cdot (x_{Max} - x)} \tag{9}$$

$$\dot{p}_5 = \frac{1}{C_{H,5}} \cdot \left(\sum_{i=1}^{4} Q_{RV,i} + Q_{EV} - Q_{POCV,1} - Q_{POCV,2} - Q_{AC,1} - Q_{AC,2} - Q_{CV,2} \right) \tag{10}$$

$$\dot{p}_6 = \frac{\beta_6 \cdot (Q_{CV,1} + Q_{POCV,2})}{V_{6,0}} \tag{11}$$

$$\dot{p}_7 = \frac{\beta_7 \cdot (Q_{CV,3} + Q_{CV,4} - Q_{EV})}{V_{7,0}} \tag{12}$$

$$\dot{p}_8 = \frac{\beta_8 \cdot Q_{EV}}{V_{8,0}} \tag{13}$$

The volumes of the transmission lines ($V_{i,0}$) are assumed constant whereas the equations related to the actuator require the piston areas, the piston position (x), and the cylinder stroke (x_{Max}). The capacitance $C_{H,5}$ used in the pressure build-up equation associated to the hydro-pneumatic accumulator is elucidated in Equation (14). Among other terms, it involves the effective accumulator gas volume ($V_{AC,0}$ = 9.2 [L]) and the pre-charge pressure of the accumulator ($p_{AC,0}$ = 0.05 [bar]).

$$C_{H,5} = \frac{V_{5,0}}{\beta_5} + \frac{V_{AC,0}}{\gamma} \cdot \frac{p_{AC,0}^{\frac{1}{\gamma}}}{p_5^{\frac{\gamma+1}{\gamma}}} \tag{14}$$

Concerning the flow rates, the contributions ascribed to the different components are clarified in the sequel. The flow rates through the POCVs ($Q_{POCV,i}$) are computed by means of the orifice Equation (15). It comprises the pressure differential across the valve (Δp_i), the discharge coefficient (C_d), the seat diameter (d_i), the poppet lift (y_i), and the fluid density (ρ).

$$Q_{POCV,i} = C_d \cdot \pi \cdot d_i \cdot y_i \cdot sign(\Delta p_i) \cdot \sqrt{\frac{2}{\rho} \cdot |\Delta p_i|} \tag{15}$$

If a POCV is not closed, two operating modes characterize its functioning. The "normal flow" condition takes place when the pilot stage is detached from the poppet. Conversely, the valve is subjected to "reverse flow" if the pilot stage and the poppet are in contact. In the case of a non-vented valve (Figure 6 depicts alternative designs), an opening pilot pressure lower than the inlet pressure is the prerequisite for "normal flow" (i.e., $p_x < p_{In}$). The poppet lift always results from the force equilibrium that is expressed differently and is contingent on "normal flow" (16) or "reverse flow" (17).

$$y_i = \frac{(p_{In,i} - p_{Out,i}) \cdot A_{S,i} - F_{S0,i}}{k_{S,i}} \tag{16}$$

$$y_i = \frac{(p_{x,i} - p_{In,i}) \cdot A_{x,i} + (p_{In,i} - p_{Out,i}) \cdot A_{S,i} - F_{S0,i}}{k_{S,i}} \tag{17}$$

The areas of the poppet seat ($A_{S,i}$) and of the pilot stage ($A_{x,i}$) are introduced in the previous equations as well as the spring stiffness ($k_{S,i}$) and the spring's pre-load force ($F_{S0,i}$). The poppet dynamics is simulated via a first-order transfer function with time constant $\tau = 0.05$ [s].

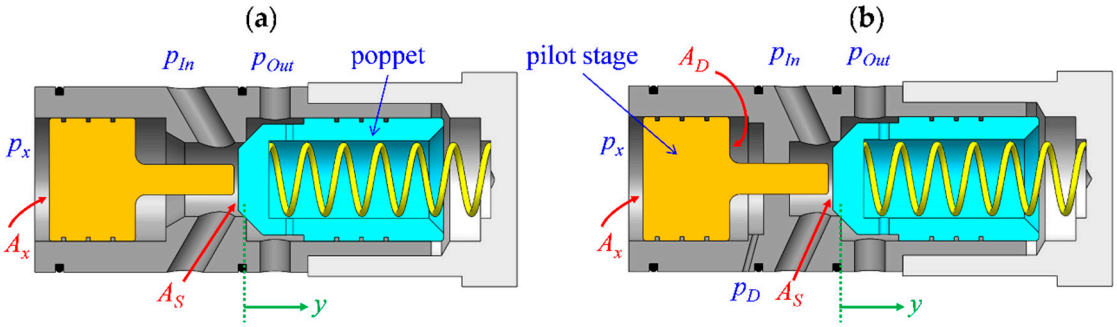

Figure 6. Cross-sectional views of pilot-operated check valves: (**a**) Non-vented design; (**b**) Vented design.

If a POCV comes in the vented version, the previous definition of the operating modes holds true, but the criterion for "normal flow" becomes $p_x \cdot A_x < p_D \cdot A_D + p_{In} \cdot (A_x - A_D)$. The force balance for the "normal flow" condition is still given by Equation (16), whereas it is described in Equation (18) for the other operating mode. The pilot stage's area inside the drain chamber ($A_{D,i}$) and the drain pressure ($p_{D,i}$) are included.

$$y_i = \frac{1}{k_{S,i}} \cdot [(p_{x,i} - p_{In,i}) \cdot A_{x,i} + (p_{In,i} - p_{Out,i}) \cdot A_{S,i} + (p_{In,i} - p_{D,i}) \cdot A_{D,i} - F_{S0,i}] \tag{18}$$

The orifice equation also provides the flow rate through the electro-valve (Q_{EV}). The only difference from the formulation given in Equation (15) is about the flow area that depends on the valve command. Then, the flow rate of both the CVs and the RVs is computed according to Equation (19).

The evoked parameters are the valve flow gain ($k_{v,i}$), the cracking pressure ($p_{c,i}$), the inlet pressure ($p_{In,i}$), and the outlet pressure ($p_{Out,i}$).

$$Q_i = \begin{cases} 0 & \text{if } p_{In,i} < p_{Out,i} + p_{c,i} \\ k_{v,i} \cdot (p_{In,i} - p_{Out,i} - p_{c,i}) & \text{if } p_{In,i} \geq p_{Out,i} + p_{c,i} \end{cases} \tag{19}$$

The effective magnitudes of the pump/motor are evaluated by means of flow losses ($Q_S \geq 0$) and torque losses ($T_S \geq 0$) derived from steady-state experimental data of a reference axial-piston unit with displacement equal to D_{Ref} [55]. The same losses are assumed for all quadrants and are scaled to the desired pump displacement (D) by using the scaling laws elucidated in Equation (20) that refer to the quantities of the reference unit denoted by the subscript "*Ref*". The scaling factor (λ), the unit's shaft speed (ω), and the losses of the reference unit are involved.

$$\lambda = \sqrt[3]{\frac{D}{D_{Ref}}} \quad \rightarrow \quad \begin{cases} \omega_{Ref} = \lambda \cdot \omega \\ Q_S = \lambda^2 \cdot Q_{S,Ref} \\ T_S = \lambda^3 \cdot T_{S,Ref} \end{cases} \tag{20}$$

The effective flow rate of the pump/motor ($Q_{e,P}$) is elucidated in Equation (21) for operations in the I quadrant and in the IV quadrant (the sign convention accounts for the functioning in pumping or in motoring mode). The flow losses are completely attributed to internal leakages.

$$Q_{e,P} = D \cdot \omega - Q_S \tag{21}$$

The computation of the pump/motor's effective shaft torque ($T_{e,P}$) expressed in Equation (22) requires the pressure differential across the unit (Δp).

$$T_{e,P} = \begin{cases} \dfrac{D \cdot \Delta p}{2 \cdot \pi} + T_S (\text{I quadrant}) \\ -\dfrac{D \cdot \Delta p}{2 \cdot \pi} + T_S (\text{IV quadrant}) \end{cases} \tag{22}$$

The pressure losses in the transmission lines and in the cooling/filtering unit are neglected mainly due to the compact configuration of the drive. Moreover, Equation (23) describes the actuator's force balance where the hydraulic force (F_H) and the friction force (F_F) are clarified in Equations (24) and (25), respectively.

$$F_H = F_F + G(x) + M(x) \cdot \ddot{x} \tag{23}$$

$$F_H = p_3 \cdot A_p - p_4 \cdot A_r \tag{24}$$

$$F_F = f_v \cdot \dot{x} + \tanh(\dot{x} \cdot a) \cdot \left(F_C + F_S \cdot e^{\frac{-\dot{x} \cdot \tanh(\dot{x} \cdot a)}{k_C}} \right) \tag{25}$$

The different terms represent the pressure in the bore-side chamber (p_3), the pressure in the rod-side chamber (p_4), the viscous friction coefficient ($f_v = 4 \times 10^3$ [kg/s]), the Coulomb force ($F_C = 75$ [N]), the static friction force ($F_S = 500$ [N]), the static friction force's constant ($k_C = 0.02$ [m/s]), the equivalent mass of the system $M(x)$, and the gravitational load $G(x)$ on the actuator. The friction in the joint of the crane is lumped into the friction of the linear actuator whereas the hyperbolic tangent is used to prevent numerical issues such as discontinuities (the dimensionless tuning parameter is set equal to a = 250). Figure 7 depicts the variation of both $G(x)$ and $M(x)$ as a function of the piston position (Appendix A); the Coriolis and the centripetal terms are neglected due to their minimal influence.

Regarding the overall system efficiency (η_{SCC}), the mechanical power at the load/actuator interface (P_C) and the servo-motor's electrical power (P_{EM}) are addressed. The latter term involves

the armature current (i_A) and the torque constant of the machine (k_T = 2.05 [N·m/A]). The ratio of the output energy over the input energy of the SCC is calculated via Equation (26).

$$\eta_{SCC} = \begin{cases} \frac{P_C}{P_{EM}} = \frac{(F_H - F_F)\cdot\dot{x}}{i_A \cdot k_T \cdot \omega} & \text{if} \quad P_{EM} \geq 0 \\ \frac{P_{EM}}{P_P} = \frac{i_A \cdot k_T \cdot \omega}{(F_H - F_F)\cdot\dot{x}} & \text{if} \quad P_{EM} < 0 \end{cases} \tag{26}$$

Diverse formulations are used if the electrical energy is supplied, or if the regenerative functioning is taking place (i.e., $P_{EM} < 0$).

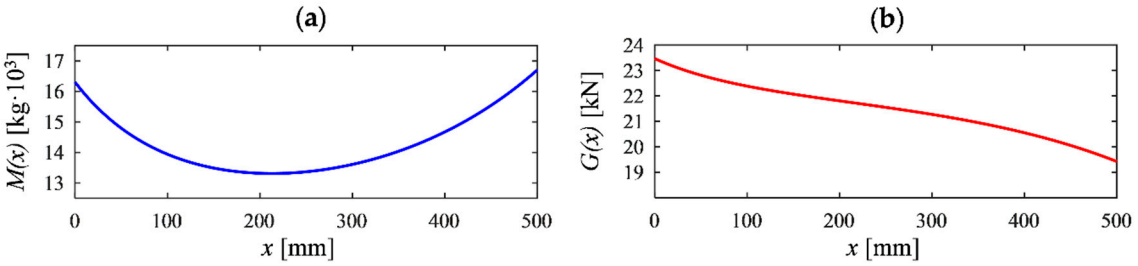

Figure 7. (**a**) Variation of the equivalent system's mass as function of the piston position; (**b**) and variation of the gravitational load acting on the actuator as function of the piston position.

5.2.Open-Loop Model Validation

The complete dynamic model of the SCC was validated against experimental data. The applied open-loop command (i.e., the desired speed for the electric motor) generates typical working conditions such as extension and retraction of the actuator. The results proposed in Figure 8 show good agreement among measured and simulated quantities, confirming the high-fidelity nature of the model. Consequently, it represents a meaningful tool for further analyses.

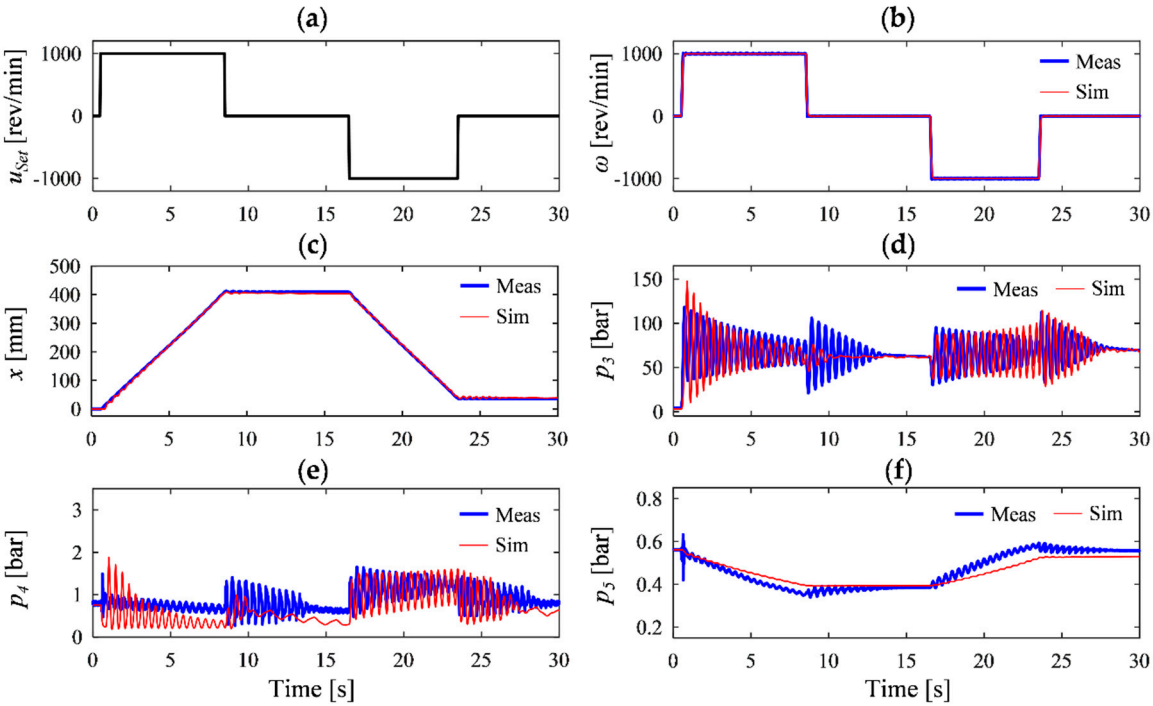

Figure 8. Experimental model validation: (**a**) Commanded motor speed; (**b**) motor speed; (**c**) piston position; (**d**) actuator's bore-side pressure; (**e**) actuator's rod-side pressure; and (**f**) accumulator pressure.

6. Closed-Loop System Performance

A representative working cycle with both active load-holding operations (A_{LH}) and passive load-holding operations (P_{LH}) serves the purpose of analyzing the system performance when the SCC is controlled in closed-loop according to the algorithm illustrated in Figure 4. The trend of the commanded position selected for this test implies a piston velocity equal to 150 [mm/s] during actuation, that represents the upper limit for the experimental set-up.

The agreement between the commanded and the measured actuator position presented in Figure 9 is satisfactory since the error falls well within ±2 [mm]. In fact, the expected accuracy for hydraulic cranes is typically worse as the maximum position error is frequently higher than 15 [mm] [56,57].

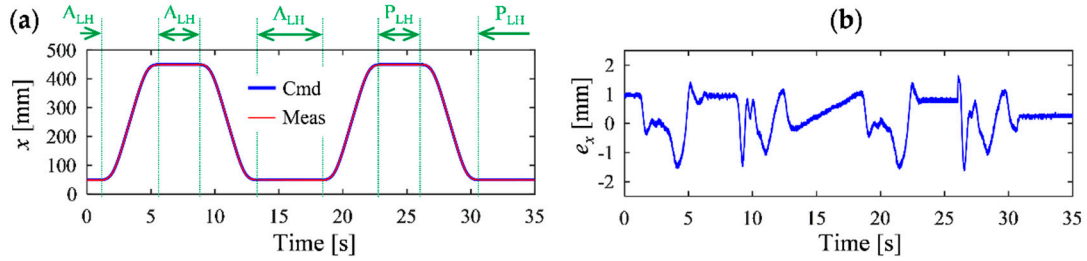

Figure 9. (**a**) Commanded and measured piston position; (**b**) Position error.

The servo-motor speed shown in Figure 10 (i.e., the control effort of this electro-hydraulic system) remains within the recommended limits of the machine (about ±3200 [rev/min]) and its variation is mostly smooth.

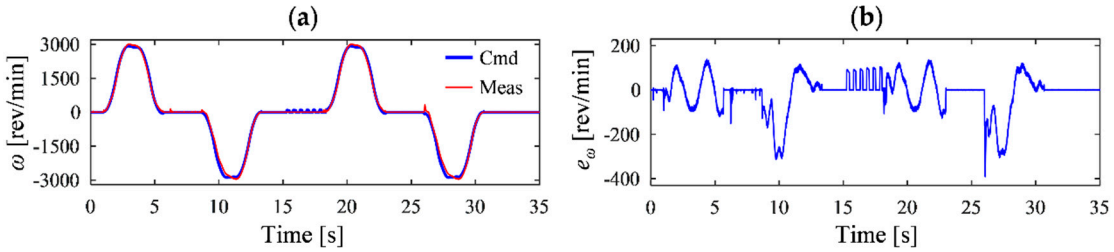

Figure 10. (**a**) Commanded and measured servo-motor speed; (**b**) Speed error.

The relevant system pressures are presented in Figure 11. They vary, as expected, showing stable behavior and smooth transitions between different operating conditions; this result is a key aspect because standard hydraulic cranes equipped with load-holding valves are usually characterized by a disturbing oscillatory behavior (this is also the case for the crane used in this investigation when powered by a conventional load-sensing system [54]). Regarding the pressures in the bore-side of the SCC, the difference between p_1 and p_3 during passive load-holding is due to the leakages across the pump/motor.

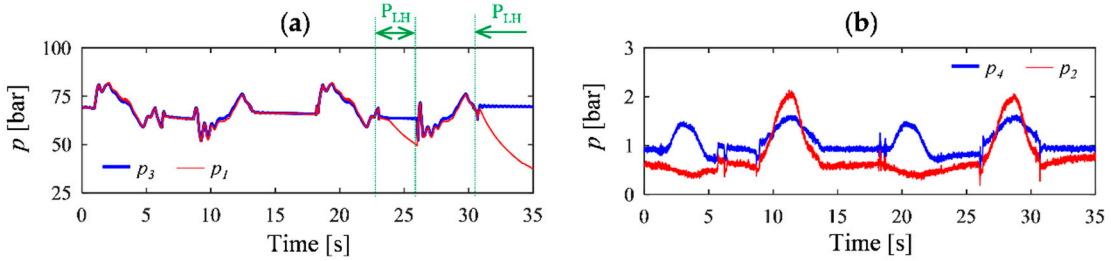

Figure 11. (**a**) Measured pressures in the bore-side of the system; and (**b**) measured pressures in the rod-side of the system.

Concerning the load-holding valves, Figure 12 highlights the poppet position and the command directed to the on/off electro-valve that supervises the load-holding devices (the passive load-holding function is activated when the signal is equal to zero).

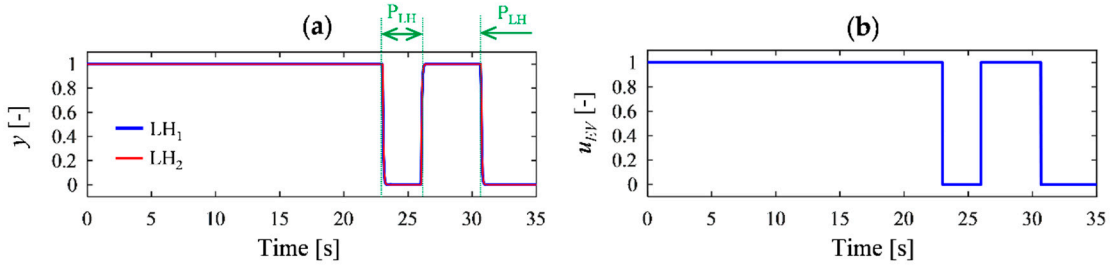

Figure 12. (**a**) Simulated poppet lift of the vented load-holding valves; (**b**) Electro-valve command.

These POCVs do not introduce any unpleasant oscillations during motion. Most importantly, they maintain the piston position when the servo-motor is not active (this is the case between about 23–27 seconds and 31–35 seconds).

Finally, the overall energy efficiency of the system is addressed in Figure 13. The average value during actuation runs in the neighborhood of 60 [%], with a slightly worse performance during regenerative functioning. This means the SCC can be considered efficient when compared to conventional valve-controlled circuits (e.g., [9]). Furthermore, the SCC is regenerating energy during piston retraction. This means the electric machine is outputting electrical energy that can be returned to the grid or can be stored in a dedicated device (in the case of the test-bed, the recovered electrical energy is dissipated by a resistor). The measured current (filtered signal) was used to calculate the electrical power, whereas a zero efficiency was arbitrarily assigned if $|P_{EM}| < 0.25$ [kW] to avoid numerical issues.

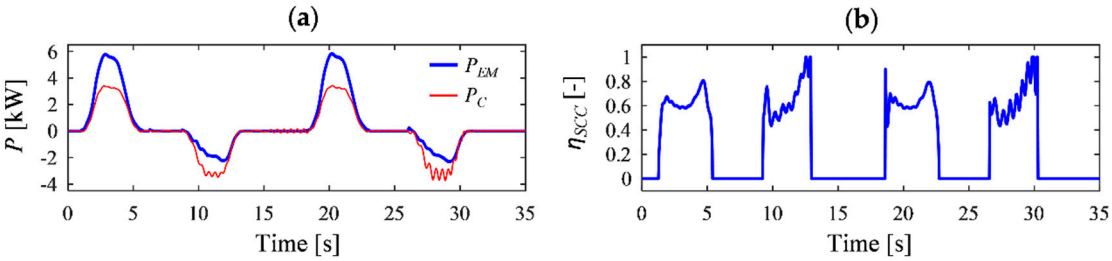

Figure 13. (**a**) Measured input power and simulated output power of the self-contained cylinder; (**b**) and simulated overall energy efficiency of the self-contained cylinder.

7. Discussion about the Load-Holding Valves

It is worth recalling that the load-holding valves represent a peculiarity of this SCC. Discussing, therefore, both their design and their arrangement is invaluable to gain deeper insight.

7.1. Design of the Pilot-Operated Check Valves

The experimental results were obtained by utilizing vented load-holding POCVs. This is the most conservative approach since the total effort required to open the poppet in a given operating condition is reduced, if compared to non-vented valves. Thus, this sub-section is about understanding how the valve design (i.e., vented or non-vented valve configuration) affects the overall system response (Figure 14).

The outcomes displayed in Figure 14 were derived by simulating non-vented load-holding POCVs where diverse values of the area ratio and of the seat diameter were considered, specifically: the "original" settings of the experimental set-up (i.e., area ratio 3:1 and seat diameter 5 [mm]), a first

alternative with area ratio increased to 7:1 and seat diameter 5 [mm], and another solution with area ratio 3:1 and seat diameter raised to 9 [mm].

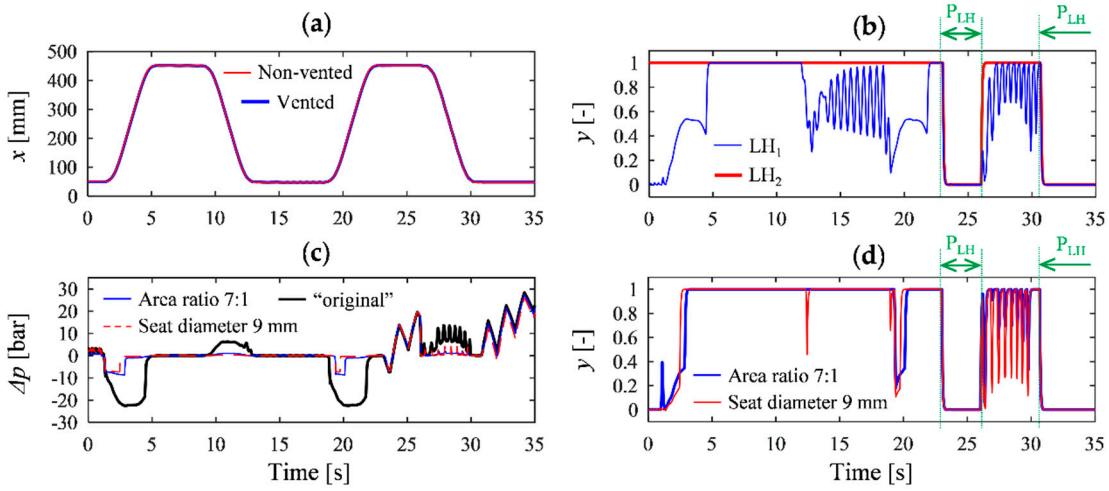

Figure 14. (**a**) Simulated piston position with vented and non-vented load-holding valves (area ratio 3:1 and seat diameter 5 [mm]); (**b**) simulated poppet lift using non-vented load-holding valves (area ratio 3:1 and seat diameter 5 [mm]); (**c**) simulated pressure drop across LH_1 using non-vented POCVs; and (**d**) simulated poppet lift of LH_1 using non-vented POCVs with modified settings.

Choosing the vented design is not strictly necessary, even though it is advisable. The piston position is, in fact, indistinguishable if non-vented POCVs are preferred to the vented counterparts (plot a) in Figure 14). Nevertheless, the poppet of the non-vented valve LH_1, located on the bore-side of the actuator, is not completely lifted from its seat when the hydraulic cylinder is actuated (plot b) in Figure 14); this aspect does not affect the position tracking, but results in an increased pressure drop across the valve that turns out in a higher energy consumption. This drawback related to energy efficiency is mitigated if non-vented load-holding valves with enlarged nominal flow (i.e., bigger seat diameter) and/or increased pilot ratio are introduced (plot c) in Figure 14). Using these modified settings, the actuator's position tracking is still equivalent to the reference scenario established by vented POCVs and the oscillations of the poppet diminish (plot d) in Figure 14).

7.2. Arrangement of the Pilot-Operated Check Valves

The other aspect that deserves further debate is the arrangement of the load-holding valves. The proposed SCC takes their opening pilot pressures from the actuator chambers, when the EV is energized. This approach is in contrast with some references that mention POCVs utilized as load-holding devices: In fact, the opening pilot pressures in these systems are taken from the pump/motor ports according to the diagram given in Figure 15.

The dynamic model of the SCC was adapted congruently to reflect the alteration in the configuration of the load-holding POCVs' pilot lines and to remove the sub-system dedicated to the selection of their pilot pressure (i.e., the EV and $CV_{3\rightarrow4}$). After simulating this transformed hydraulic architecture, it is therefore relevant to stress that such an approach leads to an unwanted system functioning when overrunning loads are acting on the actuator (Figure 16).

When the actuator load becomes overrunning between about 9.5–14 seconds and 27–31.5 seconds, then the load-holding valves do not stay open as desired (plot d) in Figure 16). This causes an oscillatory behavior that undermines both the position tracking (plot a) in Figure 16) and the operational safety. Enormous pressure fluctuations (plot c) in Figure 16) arise up to the maximum admitted value (a pressure-relief valve located on the bore-side is regulating, namely this solution is also characterized by inefficient functioning). Then, the control input (i.e., the commanded speed of the electric servo-motor) varies abruptly trying to match the commanded actuator position.

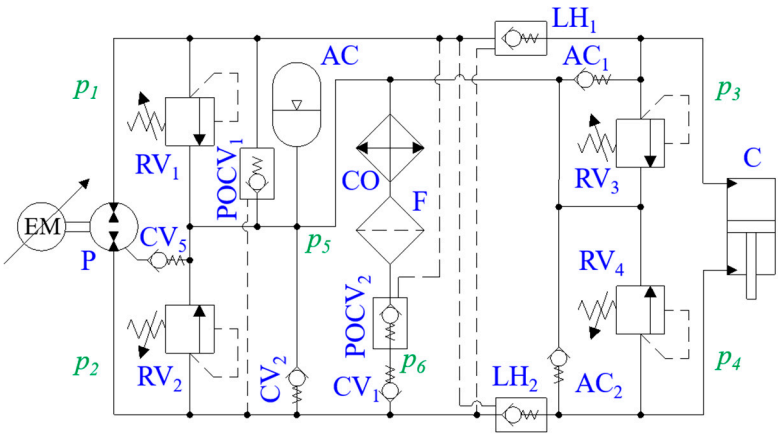

Figure 15. Alternative system with the load-holding valves arranged according to References [47–49].

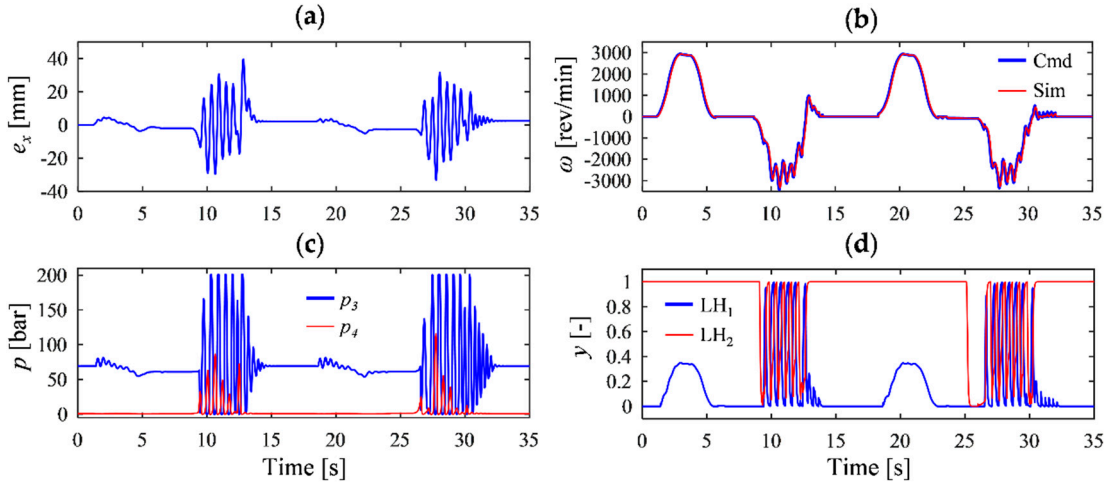

Figure 16. Simulation of the system depicted in Figure 15: (**a**) Actuator's position error; (**b**) speed of the servo-motor; (**c**) Pressures in the actuator chambers; and (**d**) poppet lift of the load-holding valves.

A similar undesirable system behavior takes place if the pilot ratio of the load-holding valves is increased (e.g., from 3:1 up to 7:1), meaning that this modified layout does not properly manage overrunning loads. Additionally, vented load-holding valves were assumed, even though non-vented components lead to equivalent results not reported for the sake of brevity.

8. Conclusions

An in-depth literature survey emphasized the need for self-contained cylinders that operate in four quadrants, include passive load-holding devices, and can deal with power levels above 5 [kW]. Consequently, this research paper gives a contribution to bridge this gap as follows:

1. A novel system architecture (i.e., a solution not found in literature) of an electro-hydraulic self-contained cylinder was presented and implemented on a test-bed.
2. Experimental evidence proves the expected system functioning; the maximum position error ranges well within ±2 [mm] and the passive load-holding capability maintains the actuator position when needed.
3. A dynamic model of the system was developed and experimentally validated; it provides a sizing and simulation tool for future implementations.
4. Insight about key parameters was given; the overall system efficiency results highly satisfactory being about 60 [%] during actuation.

5. It was shown that both vented and non-vented load-holding valves achieve the desired system functioning; however, choosing the vented design is advisable.
6. The drastic limitations caused by an alternative arrangement of the load-holding pilot-operated check valves traced in the technical literature were highlighted.

For these reasons, the proposed self-contained system can be successfully extended to several practical applications. Those including overrunning external loads and the need of securing the actuator position represent the natural field of application (e.g., cranes, presses, gripper arms for offshore pipe handling, marine jack plates, trailer lifts, scissors tables, positioning systems for solar panels, and Stewart platforms). Future work will cover the system implementation in real-world environments, the thermal analysis of this hydraulic architecture to minimize the cooler size, and considerations about the life estimation of key components. In particular, emphasis will be placed on scaling up the system to deal with higher power levels. It is expected to deliver up to about eighty [kW] by simply replacing some components with alternative off-the-shelf parts selected from the same catalogues used during the design of the experimental test-bed.

Author Contributions: conceptualization, D.P., S.K. and L.S.; methodology, D.P.; software, D.P. and L.S.; investigation, D.H.; data curation, D.P; writing—original draft preparation, D.P.; writing—review and editing, D.P., S.K. and L.S.; funding acquisition, D.H.

Funding: This research was funded by the Norwegian Research Council, SFI Offshore Mechatronics, project 237896.

Acknowledgments: The authors acknowledge the support of Bosch Rexroth: special thanks are due to Mr. Reiner Knoell (Lohr am Main, Germany) for essential inspiration and feedback during the system design and to the Norwegian branch office.

Conflicts of Interest: The authors declare no conflict of interest.

Nomenclature

Abbreviations

4Q	Four quadrant operations
A_{LH}	Active load-holding
AC	Anti-cavitation valve
C	Actuator (i.e., hydraulic cylinder)
CO	Cooler
CV	Check valve
EM	Electric servo-motor
EV	3/2 electro-valve
F	Filter
FF	Feedforward controller
LH	Load-holding valve
P_{LH}	Passive load-holding
POCV	Pilot-operated check valve
RV	Pressure-relief valve
SCC	Self-contained electro-hydraulic cylinder

Symbols

a	Tuning parameter for the friction force of the actuator and of the crane joint
A_D	Pilot stage's area inside the drain chamber of pilot-operated check valves
A_p	Cylinder area on the bore-side
A_r	Cylinder area on the rod-side
A_S	Poppet seat's area of pilot-operated check valves
A_x	Pilot stage's area of pilot-operated check valves
C_d	Discharge coefficient
C_H	Hydraulic capacitance
D	Pump/motor displacement
d	Seat diameter of pilot-operated check valves

D_{Ref}	Displacement of the reference unit used to derive the loss model of the pump/motor
e_x	Position error of the hydraulic actuator
F_C	Coulomb force of the actuator and of the crane joint
F_F	Friction force of the actuator and of the crane joint
F_H	Hydraulic force of the actuator
F_S	Static friction force of the actuator and of the crane joint
F_{S0}	Spring's pre-load force of pilot-operated check valves
f_v	Viscous friction coefficient of the actuator and of the crane joint
$G(x)$	Gravitational load acting on the actuator
i_A	Armature current of the servo-motor
k_C	Static friction force's constant of the actuator and of the crane joint
k_I	Integral gain of the PI controller
k_P	Proportional gain of the PI controller
k_{PF}	Filter gain of the high-pass pressure filter
k_S	Spring stiffness of pilot-operated check valves
k_T	Torque constant of the servo-motor
k_v	Flow gain of check valves and of pressure-relief valves
$M(x)$	Equivalent mass of the system acting on the actuator
p	Pressure
p_1	Pressure at the pump/motor port on the bore-side of the actuator
p_2	Pressure at the pump/motor port on the rod-side of the actuator
p_3	Actuator's bore-side pressure
p_4	Actuator's rod-side pressure
p_5	Accumulator pressure
$p_{AC,0}$	Pre-charge pressure of the accumulator
p_{atm}	Atmospheric pressure
p_c	Cracking pressure of check valves and of pressure-relief valves
P_C	Mechanical power at the load/actuator interface
p_D	Drain pressure in pilot-operated check valves
P_{EM}	Electrical power of the servo-motor
p_{In}	Pressure at the inlet port of hydraulic valves
p_{Out}	Pressure at the outlet port of hydraulic valves
p_x	Opening pilot pressure of pilot-operated check valves
Q	Volume flow rate
Q_d	Differential actuator's volume flow rate
$Q_{e,P}$	Effective flow rate of the pump/motor
Q_{EV}	Volume flow rate through the electro-valve
Q_p	Actuator's volume flow rate on the bore-side
Q_{POCV}	Flow rate through pilot-operated check valves
Q_r	Actuator's volume flow rate on the rod-side
Q_S	Flow losses of the pump/motor
$T_{e,P}$	Effective shaft torque of the pump/motor
T_S	Torque losses of the pump/motor
u_{EM}	Commanded servo-motor speed
u_{EV}	Command directed to the 3/2 electro-valve
u_{FF}	Commanded servo-motor speed from the feedforward term
u_{LH}	Load-holding enabler command
u_{PF}	Commanded servo-motor speed from the pressure feedback term
$V_{AC,0}$	Effective accumulator gas volume
V	Volume
x	Piston position
x_{Max}	Actuator stroke
$\dot{x}_{Set}$	Commanded piston velocity
Greek symbols	
y	Poppet lift of pilot-operated check valves
β	Effective bulk modulus of the working fluid

β_A	Air's bulk modulus
β_O	Oil's bulk modulus
γ	Adiabatic air constant
Δp	Pressure differential
ε_A	Volumetric air content of the working fluid
$\varepsilon_{A,0}$	Volumetric air content of the working fluid at atmospheric pressure
ζ	Damping term used in the servo-motor's transfer function
η_{SCC}	Overall system efficiency of the self-contained cylinder
η_v	Pump/motor's volumetric efficiency
λ	Scaling factor used in the loss model of the pump/motor
ρ	Oil density
τ	Time constant of the poppet dynamics in pilot-operated check valves
ω	Shaft speed of the pump/motor
ω_n	Natural frequency used in the servo-motor's transfer function
ω_{PF}	Cut-off frequency of the high-pass pressure filter

Appendix A

This appendix presents the specifications of the single-boom crane involved in the experimental testing. The relevant dimensions used to define the crane kinematics are highlighted in Figure A1. The boom pivots around point A whereas the actuator is connected to point B and to point C. The distances between the points A, B, C, and G (i.e., the center of mass) are evaluated via Equation (A1) whereas the effective length of the hydraulic cylinder (L_{Cyl}) is expressed in (A2).

$$L_{ij} = \sqrt{L_{ij_x}^2 + L_{ij_y}^2} \tag{A1}$$

$$L_{Cyl} = x + L_{Min} \tag{A2}$$

The equivalent mass of the system and the gravitational load acting on the actuator are elucidated in (A3) and (A4), respectively. These formulae give the trends presented in Figure 7.

$$M(x) = -\frac{4\cdot\left(L_{AG_x}^2\cdot L_{Cyl}^2\cdot m + L_{AG_y}^2\cdot L_{Cyl}^2\cdot m + L_{Cyl}^2\cdot J\right)}{\left(L_{AB} - L_{Cyl} - L_{AC}\right)\cdot\left(L_{AB} - L_{Cyl} + L_{AC}\right)\cdot\left(L_{AB} + L_{Cyl} + L_{AC}\right)\cdot\left(L_{AB} + L_{Cyl} - L_{AC}\right)} \tag{A3}$$

$$\begin{cases} G(x) = -\frac{L_{Cyl}}{L_1}\cdot\left\{2\cdot\sqrt{-L_1}\cdot g\cdot m\cdot\cos[\arccos(L_2)+\alpha]\cdot L_{AG_x} - \sin[\arccos(L_2)+\alpha]\cdot L_{AG_y}\right\} \\ \text{where :} \\ \alpha = \arctan\left(\frac{L_{AG_y}}{L_{AG_x}}\right) - \arctan\left(\frac{L_{AB_y}}{L_{AB_x}}\right) + \arctan\left(\frac{L_{AC_y}}{L_{AC_x}}\right) \\ L_1 = \left(L_{Cyl} - L_{AB} + L_{AC}\right)\cdot\left(L_{Cyl} - L_{AB} - L_{AC}\right)\cdot\left(L_{Cyl} + L_{AB} - L_{AC}\right)\cdot\left(L_{Cyl} + L_{AB} + L_{AC}\right) \\ L_2 = \frac{1}{2}\cdot\frac{L_{AB}^2 + L_{AC}^2 - L_{Cyl}^2}{L_{AC}\cdot L_{AB}} \end{cases} \tag{A4}$$

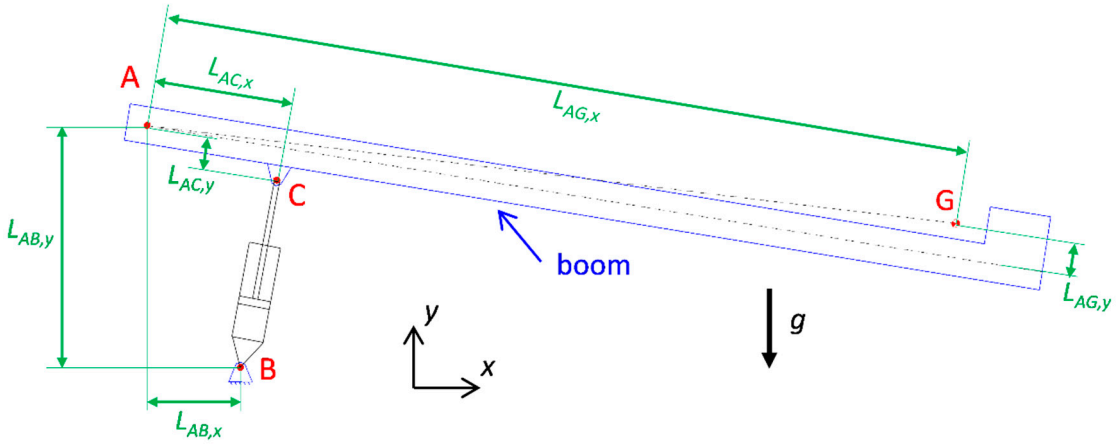

Figure A1. Kinematics of the single-boom crane used for the experimental testing.

Lastly, Table A1 collates the key parameters of the crane. These quantities are the aforementioned distances, the minimum length (L_{Min}) between point B and point C, the acceleration of gravity (g), the payload mass (m), and the moment of inertia of the crane (J) about its center of mass.

Table A1. Key parameters of the single-boom crane.

Magnitude	Value	Unit	Magnitude	Value	Unit
$L_{AG,x}$	3.139	[m]	$L_{AB,y}$	1.055	[m]
$L_{AG,y}$	0.064	[m]	L_{Min}	0.772	[m]
$L_{AC,x}$	0.550	[m]	g	9.82	[m/s^2]
$L_{AC,y}$	0.130	[m]	m	402	[kg]
$L_{AB,x}$	0.420	[m]	J	288.518	[kg·m^2]

References

1. Garcia, A.; Cusido, J.; Rosero, J.; Ortega, J.; Romeral, L. Reliable Electro-Mechanical Actuators in Aircraft. *IEEE Aerosp. Electron. Syst. Mag.* **2008**, *23*, 19–25. [CrossRef]
2. Hagen, D.; Pawlus, W.; Ebbesen, M.K.; Andersen, T.O. Feasibility Study of Electromechanical Cylinder Drivetrain for Offshore Mechatronic Systems. *Model. Identif. Control* **2017**, *38*, 59–77. [CrossRef]
3. Michel, S.; Weber, J. Electrohydraulic Compact-drives for Low Power Applications considering Energy-efficiency and High Inertial Loads. In Proceedings of the 7th FPNI PhD Symposium on Fluid Power, Reggio Emilia, Italy, 27–30 June 2012; pp. 1–18.
4. Schneider, M.; Koch, O.; Weber, J. Green Wheel Loader—Improving fuel economy through energy efficient drive and control concepts. In Proceedings of the 10th International Fluid Power Conference, Dresden, Germany, 8–10 March 2016.
5. Michel, S.; Weber, J. Prediction of the Thermo-Energetic Behaviour of an Electrohydraulic Compact Drive. In Proceedings of the 10th International Fluid Power Conference, Dresden, Germany, 8–10 March 2016.
6. Michel, S.; Weber, J. Energy-efficient Electrohydraulic Compact Drives for Low Power Applications. In Proceedings of the Fluid Power Motion Control (FPMC 2012), Bath, UK, 12–14 September 2012; pp. 93–107.
7. Weber, J.; Beck, B.; Fischer, E.; Ivantysyn, R.; Kolks, G.; Kunkis, M.; Lohse, H.; Lübbert, J.; Michel, S.; Schneider, M.; Shabi, L. Novel System Architectures by Individual Drives. In Proceedings of the 10th International Fluid Power Conference, Dresden, Germany, 8–10 March 2016.
8. Hagen, D.; Padovani, D.; Ebbesen, M.K. Study of a Self-Contained Electro-Hydraulic Cylinder Drive. In Proceedings of the Global Fluid Power Society PhD Symposium (GFPS), Samara, Russia, 18–20 July 2018.
9. Zimmerman, J.; Pelosi, M.; Williamson, C.; Ivantysynova, M. Energy Consumption of an LS Excavator Hydraulic System. In Proceedings of the ASME International Mechanical Engineering Congress & Exposition, Seattle, WA, USA, 11–15 November 2007.
10. Zimmerman, J.; Busquets, E.; Ivantysynova, M. 40% Fuel Savings by Displacement Control Leads to Lower Working Temperatures—A Simulation Study and Measurements. In Proceedings of the 52nd National Conference on Fluid Power, Las Vegas, NV, USA, 23–25 March 2011.
11. Minav, T.; Panu, S.; Matti, P. Direct-Driven Hydraulic Drive Without Conventional Oil Tank. In Proceedings of the ASME/BATH Symposium on Fluid Power & Motion Control, Bath, UK, 10–12 September 2014; pp. 1–6.
12. Altare, G.; Vacca, A. A Design Solution for Efficient and Compact Electro-hydraulic Actuators. *Procedia Eng.* **2015**, *106*, 8–16. [CrossRef]
13. Çalışkan, H.; Balkan, T.; Platin, B.E. A Complete Analysis for Pump Controlled Single Rod Actuators. In Proceedings of the 10th International Fluid Power Conference, Dresden, Germany, 8–10 March 2016; pp. 119–132.
14. Cho, S.H.; Burton, R. Position control of high performance hydrostatic actuation system using a simple adaptive control (SAC) method. *Mechatronics* **2011**, *21*, 109–115. [CrossRef]
15. Willkomm, J.; Wahler, M.; Weber, J. Potentials of Speed and Displacement Variable Pumps in Hydraulic Applications. In Proceedings of the 10th International Fluid Power Conference, Dresden, Germany, 8–10 March 2016; pp. 379–392.

16. Pedersen, H.C.; Schmidt, L.; Andersen, T.O.; Brask, M.H. Investigation of New Servo Drive Concept Utilizing Two Fixed Displacement Units. *JFPS Int. J. Fluid Power Syst.* **2014**, *8*, 1–9. [CrossRef]
17. Brahmer, B. Hybrid Drive using Servo Pump in Closed Loop. In Proceedings of the 8th International Fluid Power Conference, Dresden, Germany, 26–28 March 2012; pp. 93–102.
18. Minav, T.; Bonato, C.; Sainio, P.; Pietola, M. Direct Driven Hydraulic Drive. In Proceedings of the 9th International Fluid Power Conference, Aachen, Germany, 24–26 March 2014.
19. Schmidt, L.; Roemer, D.B.; Pedersen, H.C.; Andersen, T.O. Speed-Variable Switched Differential Pump System for Direct Operation of Hydraulic Cylinders. In Proceedings of the ASME/BATH 2015 Symposium on Fluid Power and Motion Control, Chicago, IL, USA, 12–14 October 2015.
20. Schmidt, L.; Groenkjaer, M.; Pedersen, H.C.; Andersen, T.O. Position Control of an Over-Actuated Direct Hydraulic Cylinder Drive. *Control Eng. Pract.* **2017**, *64*, 1–14. [CrossRef]
21. Ketelsen, S.; Schmidt, L.; Donkov, V.H.; Andersen, T.O. Energy Saving Potential in Knuckle Boom Cranes using a Novel Pump Controlled Cylinder Drive. *Model. Identif. Control* **2018**, *39*, 73–89. [CrossRef]
22. Croke, S.; Herrenschmidt, J. More Electric Initiative Power-By-Wire Actuation Alternatives. In Proceedings of the National Aerospace and Electronics Conference, Dayton, OH, USA, 23–27 May 1994; pp. 1338–1346.
23. Frischemeier, S. Electrohydrostatic Actuators for Aircraft Primary Flight Control—Types, Modelling and Evaluation. In Proceedings of the Fifth Scandinavian International Conference on Fluid Power (SICFP'97), Linköping, Sweden, 28–30 May 1997; pp. 1–16.
24. Kazmeier, B. *Energieverbrauchsoptimierte Regelung eines Elektrohydraulischen Linearantriebs Kleiner Leistung mit Drehzahlgeregeltem Elektromotor und Verstellpumpe*; VDI-Verl: Düsseldorf, Germnay, 1998.
25. Jun, L.; Yongling, F.; Guiying, Z.; Bo, G.; Jiming, M. Research on Fast Response and High Accuracy Control of an Airborne Brushless DC Motor. In Proceedings of the 2004 IEEE International Conference on Robotics and Biomimetics, Shenyang, China, 22–26 August 2004; pp. 807–810.
26. van den Bossche, D. The A380 Flight Control Electrohydrostatic Actuators, Achievements and Lessons Learnt. In Proceedings of the 25th International Congress of the Aeronautical Sciences, Hamburg, Germany, 3–8 September 2006; pp. 1–8.
27. Quan, Z.; Quan, L.; Zhang, J. Review of Energy Efficient Direct Pump Controlled Cylinder Electro-Hydraulic Technology. *Renew. Sustain. Energy Rev.* **2014**, *35*, 336–346. [CrossRef]
28. Rahmfeld, R.; Ivantysynova, M. Energy Saving Hydraulic Actuators for Mobile Machines. In Proceedings of the 1st Bratislavian Fluid Power Symposium, Častá-Píla, Slovakia, 2–3 June 1998; pp. 177–186.
29. Rahmfeld, R. *Development and Control of Energy Saving Hydraulic Servo Drives for Mobile Systems*; VDI-Verlag: Hamburg, Germany, 2002.
30. Williamson, C.; Ivantysynova, M. Stability and Motion Control of Inertial Loads with Displacement Controlled Hydraulic Actuators. In Proceedings of the 6th FPNI-PhD Symposium, West Lafayette, IN, USA, 15–19 June 2010; pp. 499–514.
31. Lodewyks, J. Differenzialzyliner im Geschlossenen Hydrostatischen Getriebe. *Ölhydraulik und Pneumatik* **1993**, *186*, 394–401.
32. Lodewyks, J. *Der Differentialzylinder im Geschlossenen Hydrostatischen Kreislauf*; RWTH Aachen: Aachen, Germany, 1994.
33. Vael, G.; Achten, P.; Potma, J. Cylinder Control with Floating Cup Hydraulic Transformer. In Proceedings of the Scandinavian International Conference on Fluid Power (SICFP), Tampere, Finland, 7–9 May 2003; pp. 175–190.
34. Bloomquist, J.V.; Niemiec, A.J.; Vickers Inc. Electrohydraulic system and apparatus with bidirectional electric-motor/hydraulic-pump unit. U.S. Patent 5778671A, 19 March 1998.
35. Zheng, J.; Zhao, S.; Wei, S. Application of Self-Tuning Fuzzy PID Controller for a SRM Direct Drive Volume Control Hydraulic Press. *Control Eng. Pract.* **2009**, *17*, 1398–1404. [CrossRef]
36. Wei, S.; Zhao, S.; Zheng, J.; Zhang, Y. Self-Tuning Dead-Zone Compensation Fuzzy Logic Controller for a Switched-Reluctance-Motor Direct-Drive Hydraulic Press. *Proc. Inst. Mech. Eng. Part I J. Syst. Control Eng.* **2009**, *223*, 647–656. [CrossRef]
37. Schneider, M.; Koch, O.; Weber, J.; Bach, M.; Jacobs, G. Green Wheel Loader –Development of an Energy Efficient Drive and Control System. In Proceedings of the 9th International Fluid Power Conference, Aachen, Germany, 24–26 March 2014.

38. Schneider, M.; Koch, O.; Weber, J. *Green Wheel Loader -Operating Strategy of an Energy Efficient Hybrid Drive Train*; SAE Commercial Vehicle Engineering Congress, Paper 2014-01-2400M; Rosemont, IL, USA, 2014.
39. Hewett, A.J. Hydraulic Circuit Flow Control. U.S. Patent 5,329,767A, 19 July 1994.
40. Wang, L.; Book, W.J.; Huggins, J.D. A Hydraulic Circuit for Single Rod Cylinders. *J. Dyn. Syst. Meas. Control* **2012**, *134*, 011019. [CrossRef]
41. Kenyon, R.L.; Scanderberg, D.; Nolan, M.E.; Wilkerson, W.D. Electro-Hydraulic Actuator. E.P. Patent 0,395,420A2, 31 October 1990.
42. Quan, L. Current State, Problems and the Innovative Solution of Electro-hydraulic Technology of Pump Controlled Cylinder. *Chin. J. Mech. Eng.* **2008**, *44*, 87–92. [CrossRef]
43. Zhang, D.; Li, W.; Lin, Y.; Bao, J. An Overview of Hydraulic Systems in Wave Energy Application in China. *Renew. Sustain. Energy Rev.* **2012**, *16*, 4522–4526. [CrossRef]
44. Huang, J.; Quan, L.; Zhang, X. Development of a Dual-acting AxialPiston Pump for Displacement-Controlled System. *Proc. Inst. Mech. Eng. Part B J. Eng. Manuf.* **2014**, *228*, 606–616. [CrossRef]
45. Wiens, T.; Bitner, D. An Efficient, High Performance and Low-Cost Energy Recovering Hydrostatic Linear Actuator Concept; In Proceedings of the BATH/ASME 2016 Symposium on Fluid Power and Motion Control, Bath, UK, 7–9 September 2016.
46. Cleasby, K.G.; Plummer, A.R. A Novel High Efficiency Electrohydrostatic Flight Simulator Motion System. In Proceedings of the Fluid Power Motion Control (FPMC 2008), Bath, UK, 10–12 September 2008; pp. 437–449.
47. Parker, H. Compact EHA—Electro-Hydraulic Actuators for High Power Density Applications. 2013. Available online: https://goo.gl/t2FMw2 (accessed on 17 December 2018).
48. Sweeney, T.; Kubinski, P.T.; Anderson, D.J. Electro-hydraulic Actuator Mounting. U.S. Patent 8161742 B2, 24 April 2012.
49. Rexroth, B. Advantages of Electrification and Digitalization Technology for Hydraulics. 2018. Available online: https://goo.gl/4G6Jxn (accessed on 17 December 2018).
50. Bing, X.; Xiaoping, O.; Yang, H. Energy-Saving System Applying Pressure Accumulators for VVVF Controlled Hydraulic Elevators. In Proceedings of the ASME International Mechanical Engineering Congress, Washington, DC, USA, 15–21 November 2003.
51. Altare, G.; Vacca, A.; Richter, C. A Novel Pump Design for an Efficient and Compact Electro-Hydraulic Actuator. In Proceedings of the 2014 IEEE Aerospace Conference, Big Sky, MT, USA, 2014.
52. Jalayeri, E.; Imam, A.; Tomas, Z.; Sepehri, N. A throttle-less single-rod hydraulic cylinder positioning system: Design and experimental evaluation. *Adv. Mech. Eng.* **2015**, *7*, 1–14. [CrossRef]
53. Çalışkan, H.; Balkan, T.; Platin, B.E. A Complete Analysis and a Novel Solution for Instability in Pump Controlled Asymmetric Actuators. *J. Dyn. Syst. Meas. Control* **2015**, *137*. [CrossRef]
54. Sørensen, J.K.; Hansen, M.R.; Ebbesen, M.K. Numerical and Experimental Study of a Novel Concept for Hydraulically Controlled Negative Loads. *Model. Identif. Control* **2016**, *37*, 195–211. [CrossRef]
55. Williamson, C.; Ivantysynova, M. The Effect of Pump Efficiency on Displacement-Controlled Actuator Systems. In Proceedings of the Eight Scandinavian International Conference on Fluid Power, Tampere, Finland, 21–23 May 2007.
56. Kjelland, M.B.; Hansen, M.R. Numerical and Experiential Study of Motion Control Using Pressure Feedback. In Proceedings of the 13th Scandinavian International Conference on Fluid Power, Linköping, Sweden, 3–5 June 2013.
57. Kjelland, M.B.; Hansen, M.R. Offshore Wind Payload Transfer Using Flexible Mobile Crane. *Model. Identif. Control* **2015**, *36*, 1–9. [CrossRef]